Carbon 170 (2020) 384–393

Contents lists available at ScienceDirect

Carbon

journal homepage: www.elsevier.com/locate/carbon

Research Article

The influence of H_2 and NH_3 on catalyst nanoparticle formation and carbon nanotube growth

R. Pezone [a, b, *], S. Vollebregt [a], P.M. Sarro [a], S. Unnikrishnan [b]

[a] Department of Microelectronics, Delft University of Technology, Mekelweg 4, 2628 CD, Delft, the Netherlands
[b] Dutch National Institute for Applied Scientific Research (TNO), Holst Centre, High Tech Campus 31, 5656 AE, Eindhoven, the Netherlands

ARTICLE INFO

Article history:
Received 30 April 2020
Received in revised form
22 June 2020
Accepted 17 July 2020
Available online 31 July 2020

ABSTRACT

Control of the morphology of carbon nanotubes (CNT) is fundamental for many applications. It is known that the catalyst distributions influence the vertical alignment and the height of the CNT. In this work we investigate the influence of the pre-anneal time and reductant gases, specifically NH_3 and H_2 as well as combinations thereof, on the nanoparticle (NP) formation and CNT growth. The gases H_2, NH_3 show opposite roles during the dewetting of 1 nm Fe catalyst layer. The H_2 favours uniform NP distributions (mean diameter of 15 nm) and the NH_3 forms large clusters. Playing with double annealing steps H_2- NH_3 we obtained NP with larger mean diameters $\mu = 20$ nm. We observed a mismatch between the diameters of the NP directly after annealing and the CNT after growth, due to a reshaping of the catalyst NP before the CNT nucleation. Furthermore, we found that longer annealing times decrease the CNT forest height and the H_2 exposure during the annealing improves the height and the alignment of the CNT.

1. Introduction

Application of Carbon Nanotubes (CNT) have been investigated in several fields, harvesting their benefits with respect to mechanical strength, thermal as well as electrical conductivity, high surface area etc. Lately, CNT has gained much attention from electrical energy storage or conversion applications like supercapacitors (EC), fuel cells, as well as Li-ion batteries (LIB). Traditional energy resources such as fossil fuels are disappearing over time, and because of this electric storage of energy is receiving crucial attention. The development of the batteries may seem poor in the light of Moore's law in electronics (according to which memory capacity doubles every 18 months), but it still took a revolution in materials science to achieve it. Electrical energy storage systems (EES), based on the electrochemical devices are used and optimised to support future storage demands.

Recently, much research has gone into innovating novel nano-architectures to increase the capacity and improve the lifespan of these storage devices. Currently, graphite is most commonly used as anode in the EC and LIB. They offer a very low theoretical specific capacity of 372 mA h/g and a poor ion/electron conductivity [1]. Three-dimensionally structured electrodes have been considered as suitable candidates for next-generation anode materials in order to improve these properties. Among the possible candidates, carbon nanotubes (CNT), graphene and other nanomaterials have emerged as materials of interest for the electrodes in EES. A key advantage of such materials is that the power density of the EES increases, because of a higher high electrode/electrolyte interface [1].

Of these materials, CNT are specifically of interest as they can easily be used to realize 3D carbon anodes [2]. Their theoretical electrical and thermal conductivity is about ten times that of copper, a metal generally known for its good conductivity [2]. The CNT exhibit high surface area due to their diameter range between 0.4 and 100 nm and height range of 10–1000 μm. The CNT are chemical inert, which is important for long battery lifetimes. Vertical Aligned Carbon Nanotube (VACNT) offer a higher and shorter diffusion path for Li + ions, thereby resulting in high capacity with higher charge transport within the structure compared to their 2D counterpart [3]. Considering the process of the lithiation and de-lithiation during the charge and discharge of the batteries, the ions could move in two-ways between the electrodes (from the bottom to the top of the CNT and vice versa), vertical and aligned structures promote these movements maximising the efficiency of the electrical energy storage device [4].

However, the use of the CNT as electrodes introduces challenges

* Corresponding author. Department of Microelectronics, Delft University of Technology, Mekelweg 4, 2628 CD, Delft, the Netherlands.
E-mail addresses: r.pezone@tudelft.nl, rob.pezone@gmail.com (R. Pezone).

https://doi.org/10.1016/j.carbon.2020.07.045

related to their structures. The trend that emerges from the literature is that the best performance is associated mostly to a high density and good uniformity in terms of height and straightness of the VACNT [5]. During the chemical vapor deposition (CVD) of CNT they nucleate from the metal catalyst nanoparticles (NP) and hence the distribution of these metal NP influences the CNT morphology [5–7]. The CNT grow vertically, if during the growth they are close enough together such that the Van der Waals forces cause interaction between the tubes and forces them to self-align. However, in order to achieve well controlled VACNT growth, the catalyst NP distribution play an important role.

In this paper, the control of the formation of uniform catalyst NP as function of the anneal time and the gas environment in the CVD reactor has been investigated. The goal is to develop a method to achieve straight and vertical aligned CNT only by the NP distribution. The catalyst NP formation is influenced by two different processes that occur during the dewetting: the Ostwald ripening and the subsurface diffusion of the catalyst atoms into the support layer [8,9]. Further studies have proposed that the interplay between the Ostwald ripening and the subsurface diffusion during the annealing, prior to CNT synthesis stage, in a reducing ambient is crucial to control the catalyst particle size [9]. As the Ostwald ripening proceeds, the number of particles decreases while the average catalyst diameter and the spread in the particle size distribution increases.

The formation of catalyst NP during the dewetting is also helped by reduction gases like H_2 and NH_3 as reported in literature [10]. A thermal process of catalyst thin layer like Fe, without hydrogen (or another reduction gas) does not allow the reduction of the iron oxide to iron [11], or the subsequent formation of catalyst clusters or particles [12]. Sakurai et al. annealed the NP with different flows of H_2 and they found that for low amounts of hydrogen it was insufficient to reduce the oxidized Fe thin film, and therefore no catalyst NP appear [13]. The use of H_2 is thus indispensable to invoke subsurface diffusion and the formation of nanoparticles [11].

This paper provides a systematic investigation on the influence on both annealing time and different gas es (H_2 and/or NH_3) on NP formation and the subsequent CNT growth. Distinct differences in NP formation between both gases were observed, which reflect to the dimension of the NP. We found a higher diameter uniformity for the H_2 annealed NP, compared to a catalyst film annealed in NH_3 or NH_3+ H_2. Lastly the use of H_2 as annealing gas leads to the formation of the smaller NP than H_2+ NH_3 and NH_3.

2. Experimental

The sample used consists of two e-beam deposited thin-films on a 6″ Si (100) wafer. The intermediate layer which supports the catalyst is Al_2O_3 (20 nm) and the catalyst layer is Fe (1 nm). The e-beam depositions have been performed by Philips Innovation Services (PInS) with a Balzers BAK 550. Squared samples of 1 cm × 1 cm cut from the same 6″ wafer were used for all CVD runs to minimize possible variations of the deposition process on the observed results. The annealing and growth steps have been done in a commercially available AIXTRON Black Magic Pro CVD reactor. Each square sample is placed at the centre of the circle chuck in the reactor. Our CNT growth process consists of an annealing phase, followed by growth using C_2H_2 (50 sccm) as the carbon source for 100 s, together with 700 sccm of H_2. The gas flows in the recipe are based on previous work that demonstrated the ability to grow tall and aligned CNT using Fe on Al_2O_3 under these conditions [14]. The substrate holder temperature during the growth-phase is 600 °C. Here, we focused only on varying the annealing process by using two different reduction gases H_2 and NH_3 with the same amount of flow (700 sccm) for different times (10, 60, 300 s). For the three gas combinations H_2 (700 sccm), NH_3 (700 sccm), H_2 + NH_3 (350 sccm + 350 sccm), we set the annealing temperature at 500 °C for three different times 10, 60, 300 s to investigate also the effect of the time on the NP formation. The pressure is fixed at 80 mbar for all experimental runs. All experimental runs are summarised in Table 1.

The annealing gas is already inserted during the ramp up phase of the heater (~200 s) and remains till the end of the annealing process. The annealing time specified in the table starts when the temperature has reached 500 °C. To further study the effect of both gases on the morphology of the NP during the annealing, we furthermore performed five two-steps annealing runs (runs 10–14, Table 1). For ex. in runs 12–14, we expose the catalyst thin layer for 10, 25, or 50 s to NH_3 (700 sccm) followed by a second step of 300 s H_2 (700 sccm).

To analyse the morphology of the NP a NT-MDT NTEGRA Atomic Force Microscopy (AFM) was used. All inspections have been done in a semi-contact mode. The cantilever used was the “NSG10” Golden Series by Techno-nT (tip curvature between 6 and 10 nm). The AFM data of the catalyst NP are characterised by Gwyddion 2.50 and Matlab tools. Finally, the CNT were inspected using a FEI Nova Nanosem 600.

3. Results and discussion

3.1. Single-step annealing results

Fig. 1 summarises the effects of the annealing gas and time on the dewetting of the NP. It shows the AFM inspections obtained after the annealing steps by the three different gases: H_2, H_2 + NH_3, NH_3 (runs 1–9 – Table 1).

From the AFM inspections, the mean diameters (assuming a normal distribution) of the NP are shown in Fig. 2. It also includes the measurements related to the double step annealing (Table 1 runs: 10, 11, 12, 13, 14) described below. We confirm that the hydrogen is crucial to break down the Fe thin film into small NP as reported in literature [13,15–18]. This trend occurs regardless of the annealing time (10, 60, 300 s). From Figs. 1 and 2 it is apparent that large NP and clusters appear for the NH_3 + H_2 or NH_3 exposure, and consequently H_2 is more suitable to realize smaller and more uniform distributions of the catalyst NP [13]. The ability of H_2 to form separated and well-defined NP is also confirmed by the anneal with both H_2 (350 sccm) and NH_3 (350 sccm). If we compare these NP with the clusters made by only NH_3 (700 sccm), the addition of H_2 improves the formation of smaller and well-defined NP. The H_2 during the annealing increases the subsurface diffusion of the Fe atoms in the Al_2O_3 support layer reducing the dimensions of the

Table 1
Lyst of the performed experiments. Runs 10–14 (two-steps annealing).

RUN N.	Time [s]	Gas	Flow[sccm]
1	10	H2	700
2	60	H2	700
3	300	H2	700
4	10	H2, NH3	350, 350
5	60	H2, NH3	350, 350
6	300	H2, NH3	350, 350
7	10	NH3	700
8	60	NH3	700
9	300	NH3	700
10	60 + 60	NH3 + H2	700
11	60 + 60	H2 + NH3	700
12	10 + 300	NH3 + H2	700
13	25 + 300	NH3 + H2	700
14	50 + 300	NH3 + H2	700

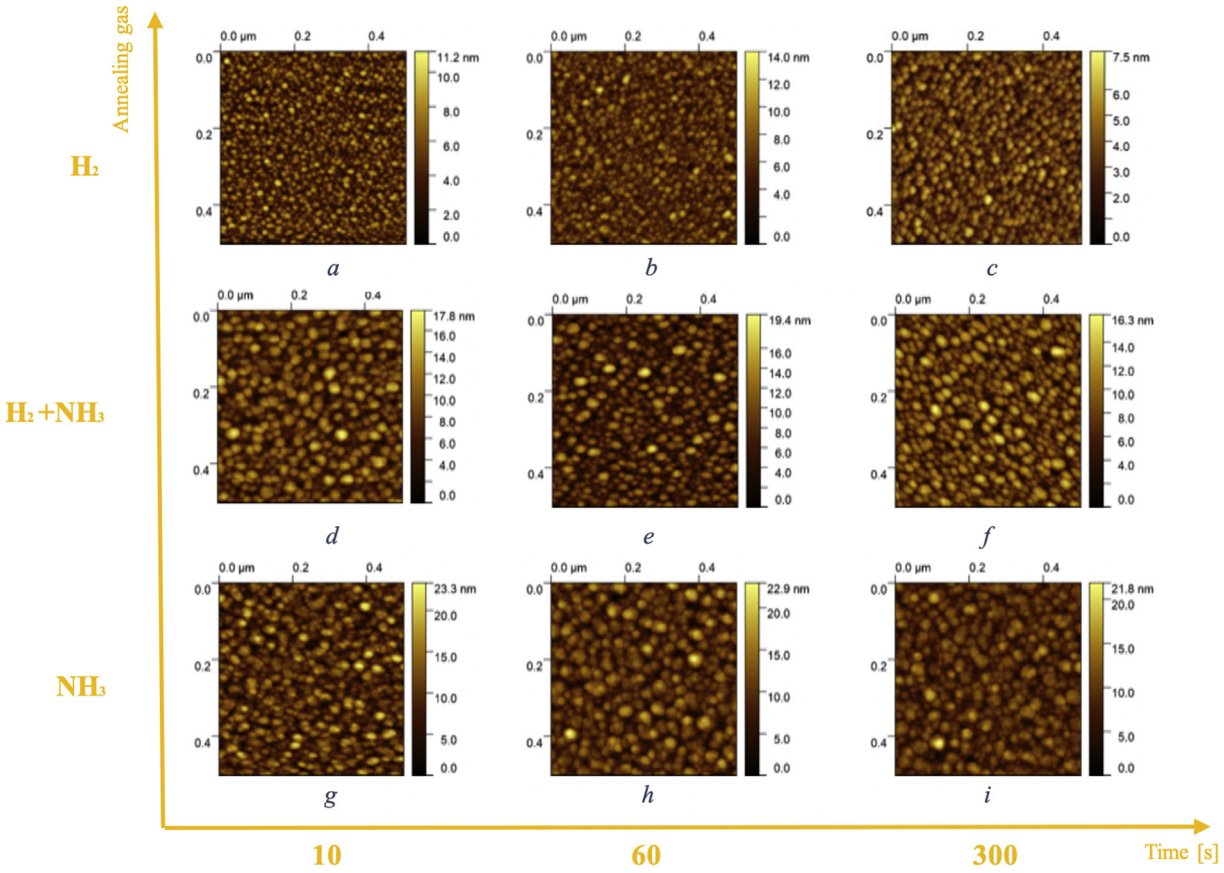

Fig. 1. AFM images. 500 nm × 500 nm scanned area. The NP are related to the experimental processes showed in Table 1. (A, b, c) run 1, 2, 3. (D, e, f) run 4, 5, 6. (G, h, i) run 7, 8, 9. (A colour version of this figure can be viewed online.)

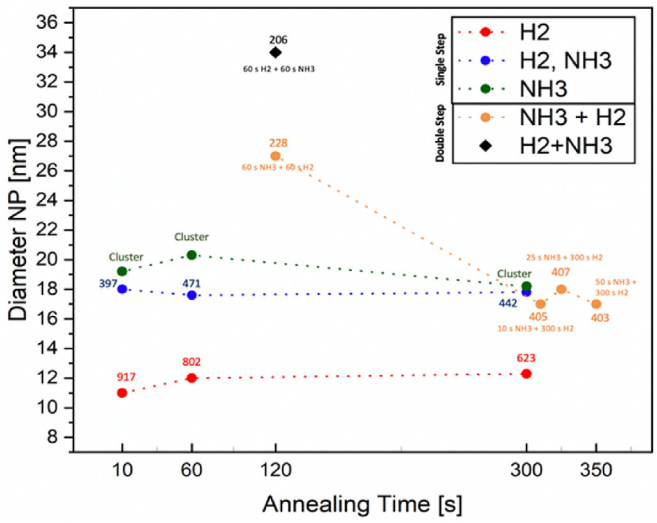

Fig. 2. Mean diameter (normal distributions) of the AFM results related to the runs 1–14 (Table 1). The number of the NP counted in the 500 nm × 500 nm AFM image is shown by the numerical value above the data points. (A colour version of this figure can be viewed online.)

catalyst NP [6,8–10,13,19,20]. The Ostwald ripening effect appears when the annealing time is increased and the NP are exposed to H_2. The catalyst NP become bigger reducing their number from 917 NP (10 s) to 623 NP (300 s) as reported in Fig. 2. Continued annealing in the presence of H_2 allows the clusters to coarsen. This process, driven by surface energy minimization, occurs through transport of Fe among the clusters.

The external atoms of the smallest NP have an excess energy w. r. t. the bulk and they are facilitated to move to the big NP in order to reduce the excess energy. This trend does not occur equally for the other inspections (H_2 + NH_3, NH_3 in Fig. 1d – i). For the H_2 + NH_3 annealed NP, the number of particles does not significantly change according to the small variation of the dimensions of catalyst NP. We observe 397 NP (10 s), 471 NP (60 s) and 442 NP (300 s) (Fig. 2). A direct proportional connection between the time of annealing with H_2 + NH_3 exposure and the number of NP was not found. It must be noted that the number and the dimensions of NP for the NH_3 anneal processes cannot be as precisely determined as for the H_2 and H_2 + NH_3 processes because they are not well-defined NP but instead form clusters. For the H_2 and H_2 + NH_3 processes, the NP appear as a distinct feature in the AFM height profile (Fig. 3a).

However, for the NH_3 runs, clusters of NP are formed instead of single NP (Fig. 3b), which makes the determination of individual NP less reliable. We have summarised these differences in Fig. 4. The dewetting of our thin catalyst layer of Fe (1 nm) with NH_3 (700 sccm) forms big clusters and we have found different height peaks in the profile of one big cluster (Fig. 3b).

These results are different from the H_2 and H_2 + NH_3 annealed NP where there are single height peaks for each NP (Fig. 3a). When the NP are bigger ($\mu = 20$ nm), with the increasing of time from 10 to 300 s the subsurface diffusion dominates the Ostwald ripening. Furthermore, the use of H_2 + NH_3 could provide a balance between

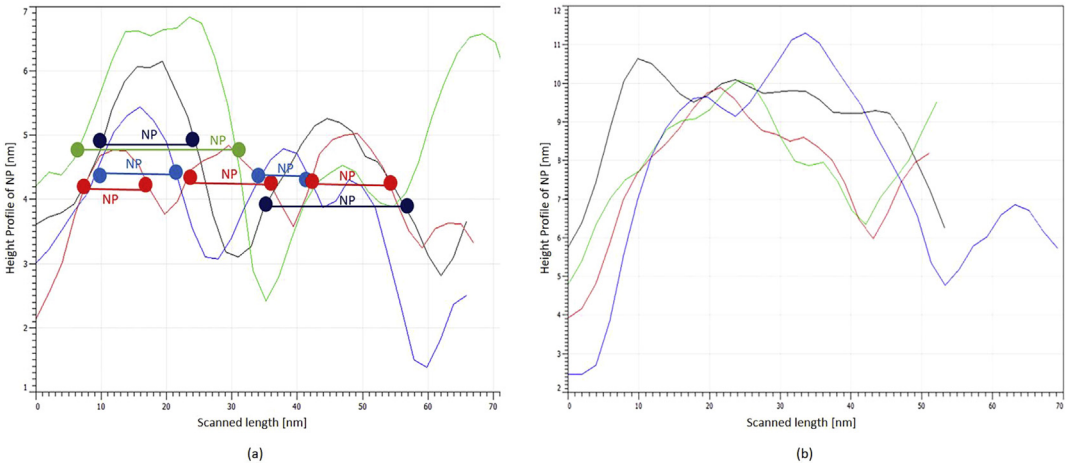

Fig. 3. Height profiles of the catalyst NP. (A) H_2 annealed NP (one height peak for each NP), (b) NH_3 annealed NP (several peaks for each cluster - not defined NP). (A colour version of this figure can be viewed online.)

Fig. 4. The catalyst NP determined by the three annealing gases (H_2, H_2 + NH_3, NH_3). (A colour version of this figure can be viewed online.)

the subsurface diffusion and the Ostwald ripening, because the diameter changes less than the other cases (Fig. 2). In this case the atoms of the big NP (H_2 + NH_3) are already more stable, so the Ostwald ripening does not occur as rapidly. Another theory would suggest that H_2 and NH_3 have the opposite effect on the morphology of the NP, so that they would counteract each other. In Fig. 5 the normal distributions of the diameter of the catalyst NP are plotted. The use of H_2 determines the highest uniformity for our NP and consequently we expect straighter and more aligned CNT than the other samples (H_2 + NH_3, NH_3). When the mean value of the diameter of the NP increases, the uniformity of the catalyst NP decreases.

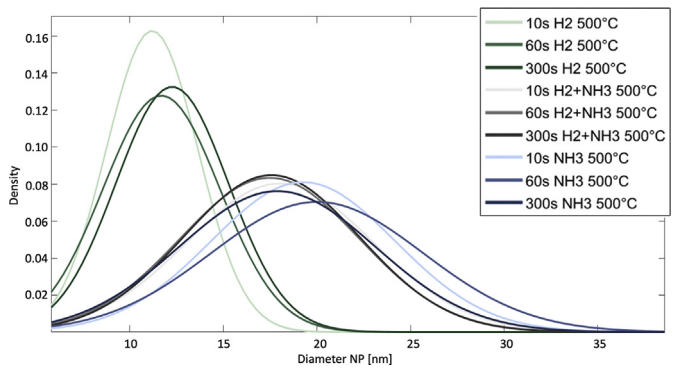

Fig. 5. Normal distributions of the diameters of the NP. Annealing conditions: tab.1 (1, 2, 3, 4, 5, 6, 7, 8, 9). (A colour version of this figure can be viewed online.)

3.2. Two-step annealing results

In order to demonstrate the opposite effects of H_2 and NH_3 gases during the dewetting we have performed a two-step annealing (Fig. 6). We want to investigate if the H_2 exposure could also form small well-defined NP starting from big clusters formed by NH_3 annealing, and vice versa.

In this way we could potentially open up a new way to control the dimension of the catalyst NP by using different annealing steps with different gases. In Fig. 6a – d, the effects of the two annealing steps are summarised. The results confirm our prediction about the effects of the H_2 and NH_3 on the morphology of the catalyst NP. The H_2 (700 sccm) annealed NP for 60 s at 500 °C have as mean value of the diameter 11 nm (Fig. 6e). With the double step of annealing, starting with H_2 annealed NP we run a second step with NH_3, and the NP increase their mean value of the diameter from 11 nm to 34 nm forming large clusters (Fig. 6f). The amount of NP changes from 802 NP (60 s H_2) to 206 NP (60 s H_2 + 60 s NH_3). In the opposite case we form well defined big NP of 27 nm of the mean diameter (Fig. 6d), so the clusters illustrated in Fig. 6c disappear. We have confirmed that the diffusion is favoured by the H_2 exposure. The H_2 forms well defined and smaller NP. To further study this effect we decreased the NH_3 (first step) exposure and we increase the time of H_2 to a fixed 300 s (Table 1, run nr. 12, 13, 14). First the NH_3 step is set for 10, 25, 50 s because we first want to form big clusters and see if they decrease forming well defined NP at a later stage when exposed to H_2. We expect the number of NP would increase for the long H_2 exposure. The AFM inspections confirm this trend because the number of NP increases dramatically for a two-step process with longer H_2 exposure (Table 2). Interestingly, the time of the NH_3 exposure has no influence on the number of NP, indicating that the H_2 step is sufficiently long to counteract the clustering due to the NH_3 exposure.

3.3. CNT growth results

The growth recipe uses C_2H_2 (50 sccm) and H_2 (700 sccm) for 100 s at 600 °C. We anneal the samples and grow the CNT in one single run. The role of the catalyst NP during CNT growth is not completely understood, but the nanoparticles could act as dynamic templates dictating the nanotube size distributions [21,22]. The appropriate density and uniformity of nanoparticles on the substrate is crucial in growing vertically aligned CNT [18]. From our results, the heights of the CNT decrease with the increasing of the

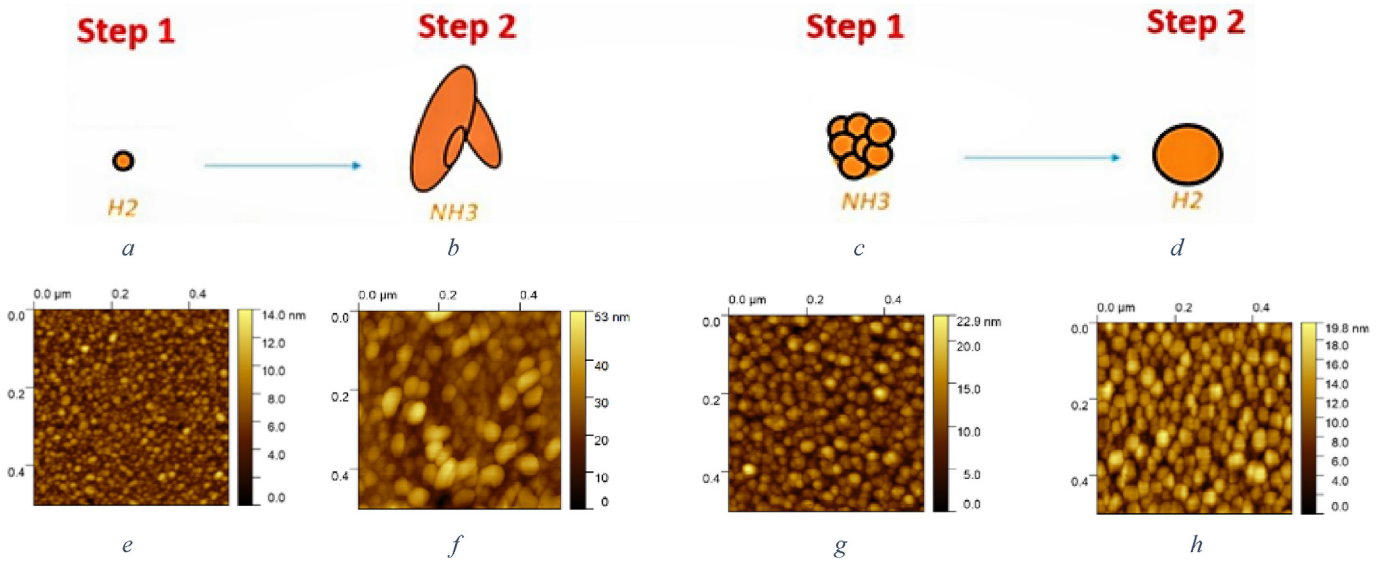

Fig. 6. Two annealing steps. First step: H_2 (700 sccm), 60 s, 500 °C (a, e). Second step: NH_3 (700 sccm), 60 s, 500 °C (b, f). First step: NH_3 (700 sccm), 60 s, 500 °C (c, g). Second step: H_2 (700 sccm), 60 s, 500 °C (d, h). (A colour version of this figure can be viewed online.)

Table 2
Number of the NP (two-step annealing process).

Annealing Conditions	(60 s) NH_3 + (60 s)H_2	(10 s) NH_3 + (300 s) H_2	(25 s) NH_3 + (300 s) H_2	(50 s) NH_3 + (300 s) H_2
Number of the NP	228	405	407	403

annealing time (10–300 s) independently of the type of the annealing gas used (H_2, NH_3, H_2+ NH_3) as described in Fig. 7, except for the last three double annealing steps (Table 1, run 12, 13, 14). In this case the H_2 exposure during the annealing prevails over the first NH_3 exposure leading to higher CNT.

The height of the CNT related to the H_2 annealed samples changes from 80 μm to 63 μm when the annealing time increases from 10 s to 300 s (Fig. 8a and b). Considering the same annealing time with H_2 + NH_3 exposure, the heights of the CNT are 36 μm and 28 μm, respectively. The CNT growth on the annealed NH_3 clusters shows the heights of 19 μm and 14 μm for 10 s and 300 s of annealing (Fig. 8c, d).

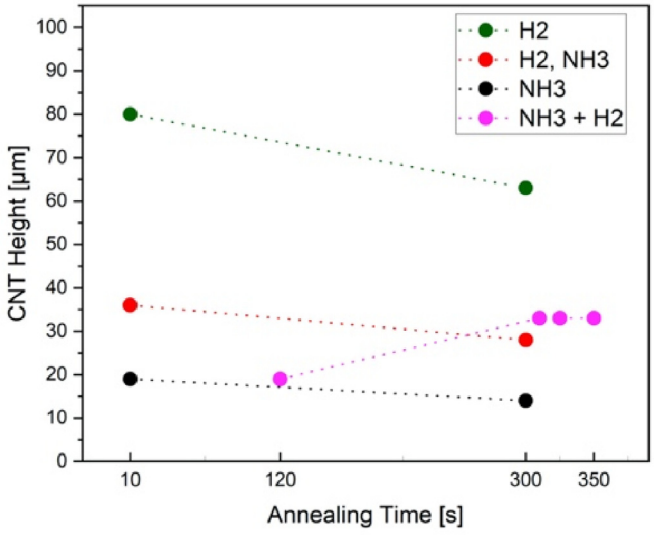

Fig. 7. CNT heights for a constant growth recipe (700/50 sccm H_2/C_2H_2, 600 °C, 100 s) and different NP annealing conditions. The annealing conditions can be found in Table 1(runs 1, 3, 4, 6, 7, 9, 10, 12, 13, 14). (A colour version of this figure can be viewed online.)

By inspecting close-ups of the bundles we can determine the diameter and vertical alignment of the CNT (Fig. 9a – d). We observe that the alignment appears to be improved when the annealing time increases from 10 s to 300 s for the H_2 only exposure. The diameters of the CNT related to the annealing with H_2 for 300 s are larger than those obtained for the annealing of 10 s. The diameter range of the CNT which is 8.8 – 14.6 nm for 300 s anneal, compared to 7.3 – 11.6 nm for the CNT related to the 10 s H_2 anneal. These differences are consistent with the larger dimensions of the 300 s H_2 catalyst NP as observed by AFM compared to the 10 s H_2 annealed NP (Fig. 2). From Fig. 9a – d, the CNT related to the 300 s H_2 look straighter than the 10 s H_2 NP. Interestingly, the straightness of the CNT doesn't improve their height (Fig. 7).

The observed different in height could originate from a difference in growth speed. It is known that larger CNT grow slower than the thinner CNT [23]. The diffusion time for carbon atoms to arrive at the growth site would become shorter for the smaller NP, resulting in accelerated growth rate of the CNT [23]. Besides, less carbon will be required to form the CNT. Comparing the previous two CNT distributions in Fig. 9c, d, we note more bundles of the CNT for the 300 s annealed NP than the 10s H_2 NP. It seems these bundles could improve the alignment of CNT (Fig. 10 – red circles) thanks to the high crowding effect of the dense packed CNT [24].

For the H_2 + NH_3 and NH_3 annealed NP the previous mentioned correlation between NP size and diameter does not appear to hold, as we do not observe CNT with larger diameters (Fig. 11d – f). The heights decrease when we use H_2 + NH_3 or NH_3, and from Fig. 11a – c we see that the NH_3 only annealed CNT appear to have the least alignment. Several mechanisms can account for this. For instance, the big clusters don't form CNT because the size of big NP is much

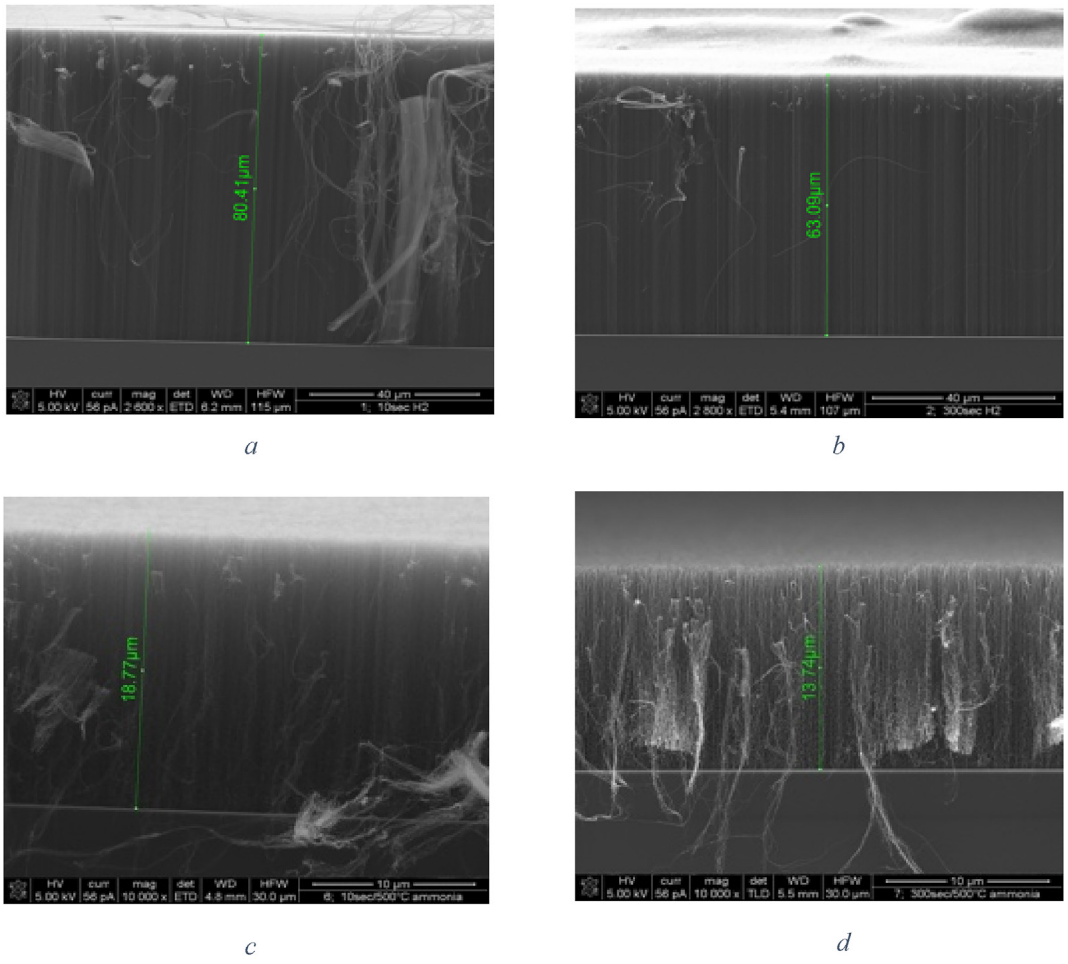

Fig. 8. SEM Cross-Section images. CNT heights. Annealing conditions: Table 1 (1, 3, 7, 9). A (run 1), b (run 3), c (run 7), d (run 9). (A colour version of this figure can be viewed online.)

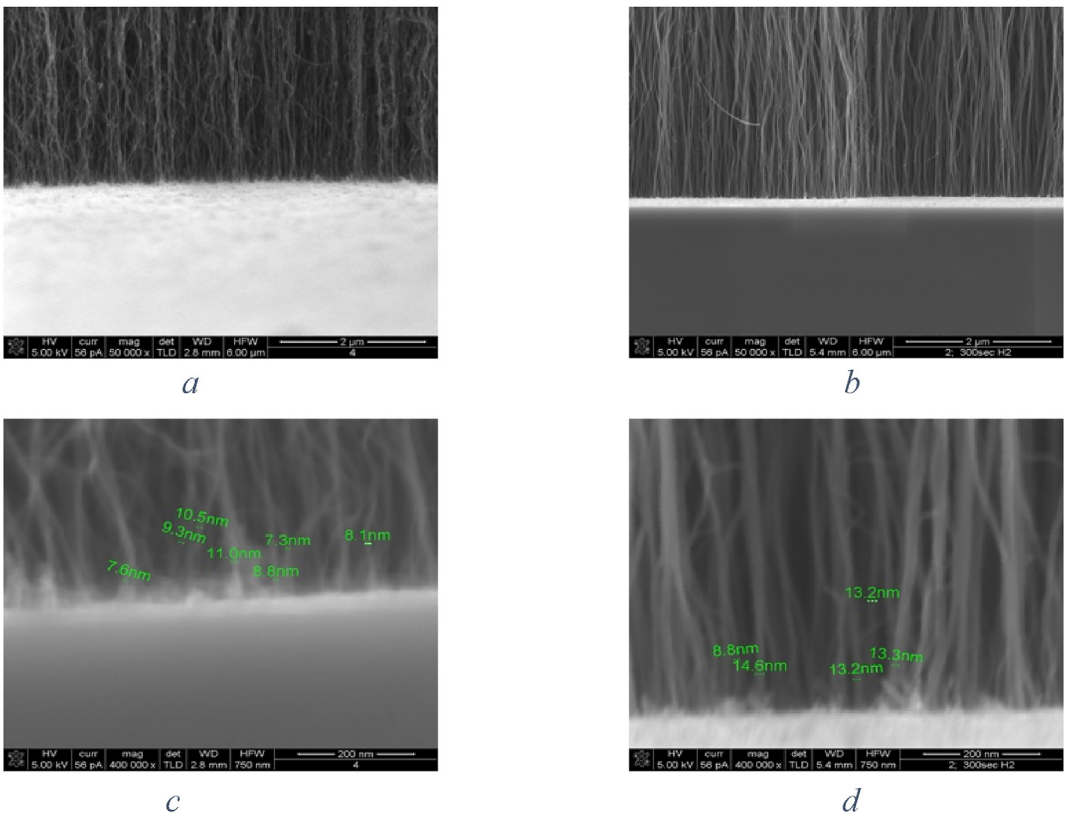

Fig. 9. SEM Cross-Section images. Diameter and alignment measurements of CNT. Annealing conditions: Table 1 (1, 3). A (run 1), b (run 3), c (run 1), d (run 3). (A colour version of this figure can be viewed online.)

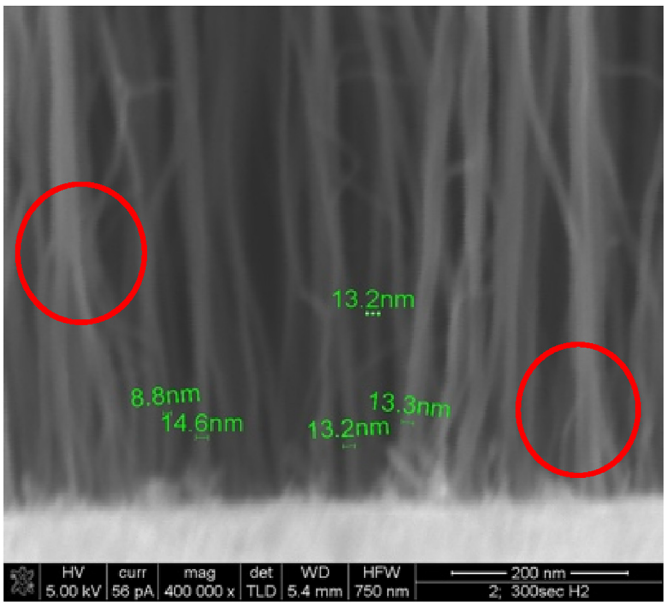

Fig. 10. SEM Cross-Section image. Annealing condition: Table 1 (Run 3). (A colour version of this figure can be viewed online.)

larger than the diffusion length of C atoms [23]. Alternatively, the larger NP are inactive due to "underfeeding" phenomenon [25]. It also could be possible that the NH_3 exposure favours the doping of Fe NP resulting in the formation of FeN, which according to literature is possible at the annealing temperature of 500 °C [26]. It has been shown that the incorporation of nitrogen into the catalyst can influence the phase of the Fe nanoparticles and the structure of the resulting CNT [27].

We formulate another suitable explanation for the shorter CNT, and the incongruity between the CNT and the NP diameters. It can be related to the reshaping of the catalyst NP before or during the exposure of C_2H_2. The big clusters larger than 15 nm (annealed $H_2 + NH_3$ and NH_3) need a period of the time to reshape in small NP (5 nm − 15 nm). Later, they start to grow and consequently the height is shorter as the affective growth time has been reduced. The CNT growth by the $H_2 + NH_3$ annealed NP is higher than the NH_3 annealed NP, because they are related to clear/single NP and they are smaller than the NH_3 NP clusters. Following this assumption, for our experiments, the CNT grow only on the catalyst NP smaller than 15 nm because we didn't observe CNT with larger diameters. For the CNT growth related to the double step of annealing with NH_3 and H_2 exposure (60 s + 60 s and 10, 25, 50 s + 300 s) we expect to see that the CNT are shorter than the single H_2 annealing step and their diameters are smaller than the ones of the original catalyst NP confirming the reshaping. Looking at the images in Fig. 12 a, b, c we can confirm the benefit of H_2 during the annealing on the next growth of CNT (straighter and higher). By this way the last step with H_2 can dominate and cancel the effect of the NH_3 exposure avoiding less well-aligned CNT.

As can be seen in Fig. 7 the CNT forest heights are comparable as those of the recipes using a combination of NH_3 and H_2. Once again, we didn't find a relation between the NP and the CNT because we haven't had CNT with diameters larger than 12–13 nm. These CNT are shorter than the 300 s H_2 even if they show the same kind of alignment and straightness. They are shorter because the bigger NP reshape before the growth and when they have the suitable dimensions, the CNT start to grow. In Fig. 13 we show our model of what occurs during the growth process. We start with big NH_3 annealed clusters (first step) and they organise themselves in big NP with the exposure of H_2 for 300 s. During the growth the particles reshape into smaller NP which correspond to the CNT diameters. Due to the proximity of the CNT they form well aligned

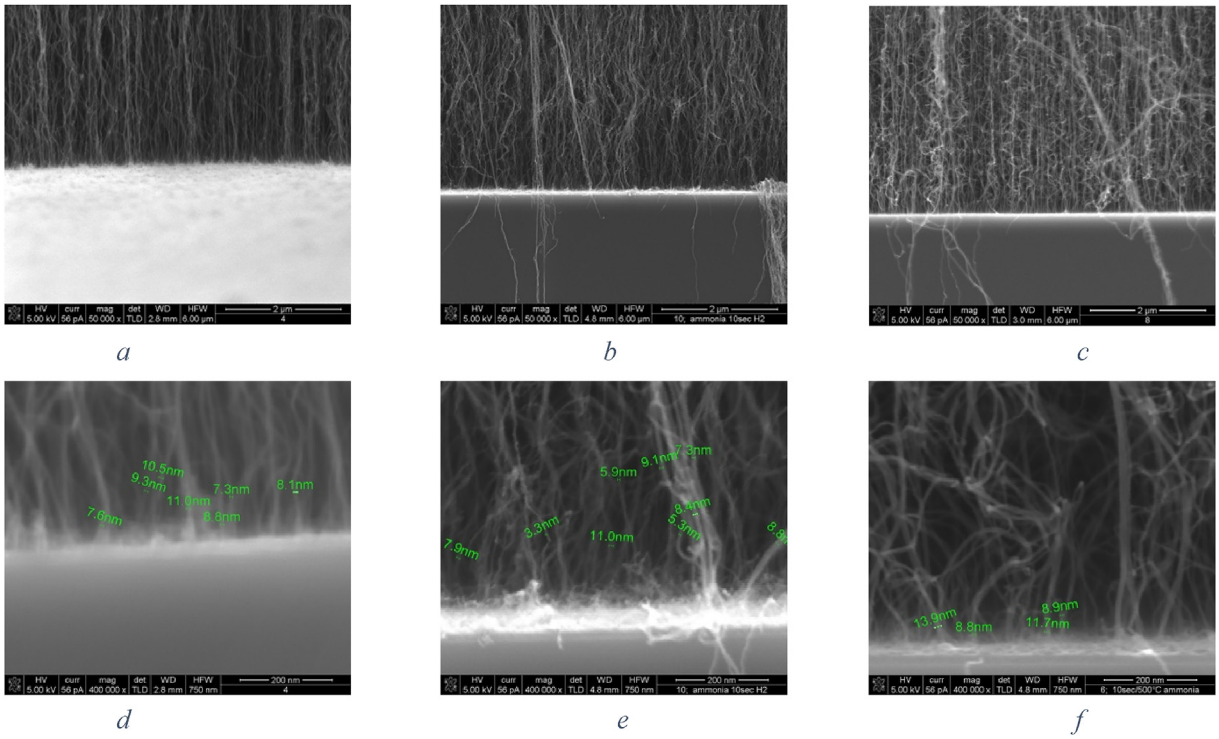

Fig. 11. SEM Cross-Section images. Diameter and alignment inspections of CNT. Annealing conditions: Table 1(1, 4, 7). (A, d) run 1. (B, e) run 4. (C, f) run 7. (A colour version of this figure can be viewed online.)

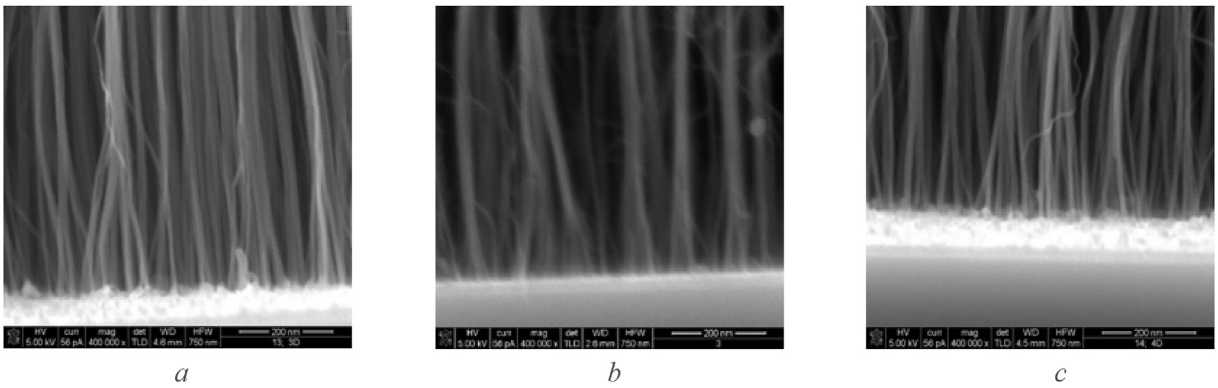

Fig. 12. SEM Cross-Section images. Annealing conditions: Table 1 (12, 13, 14). Two annealing steps: (A) run 12. (B) run 13. (C) run 14.

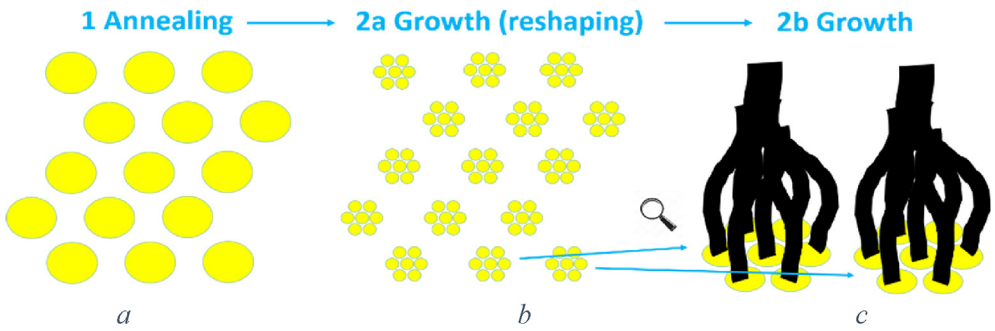

Fig. 13. The reshaping of catalyst NP after the annealing steps. (A) Catalyst NP after the annealing step. (B) The reshaping of catalyst NP during the exposure of C_2H_2. (C) The growth of CNT. (A colour version of this figure can be viewed online.)

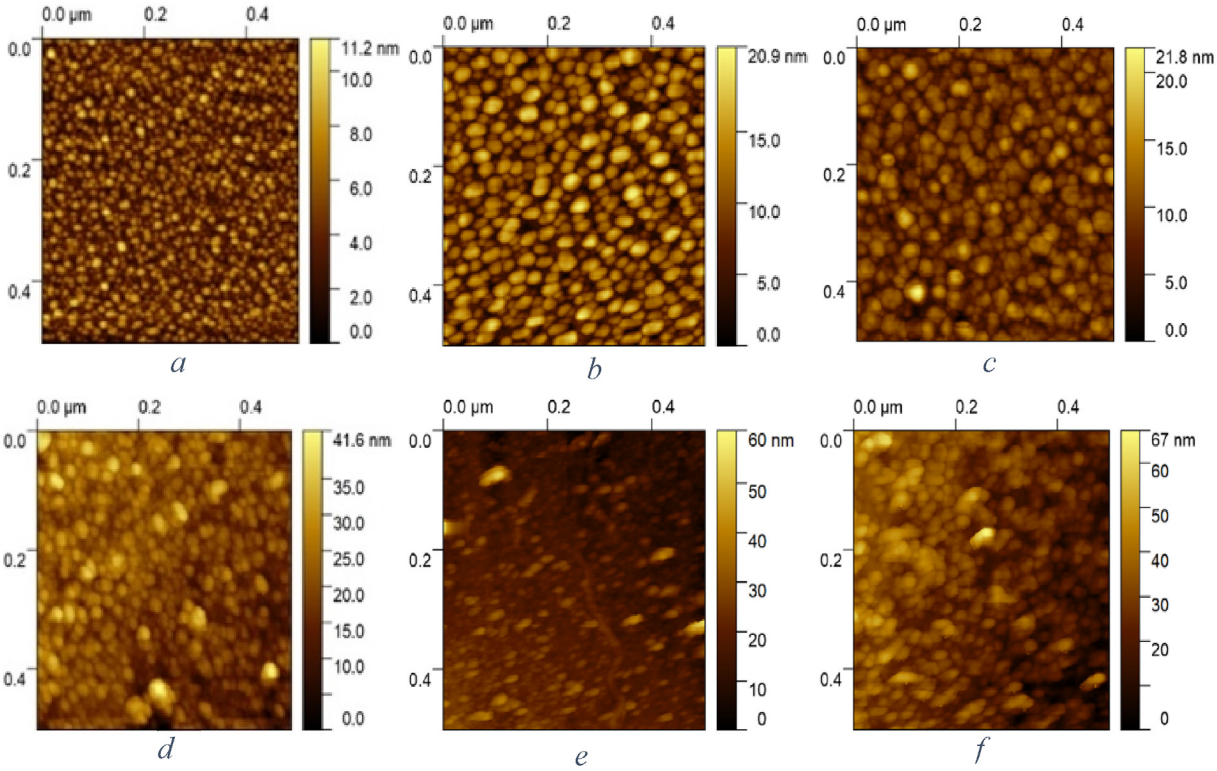

Fig. 14. AFM inspections of catalyst NP. 1st row: before the growth. 2nd row: after the growth. Area analysed 500 nm x 500. (A, d) Run 1. (B, e) Run 12. (C, f) Run 9. (A colour version of this figure can be viewed online.)

bundles. During growth the reduction gas was continuously set to H_2. This choice appears advantageous for the alignment and the height of CNT. Looking at Fig. 7, exposing the 60 s NH_3 cluster to H_2 at 500 °C for 60 s, the second exposure wasn't enough to shrink the NP compared to 300 s of H2 as shown in Fig. 2. Therefore, the CNT show shorter heights than the 10, 25, 50 s + 300 s H_2 annealed NP, confirming again the reshaping and the shrinking of the NP during the first part of the C_2H_2 exposure. Having found the way to control the dimension of catalyst NP, we haven't seen the consequent modulation of CNT diameter, i.e. the correlation between the diameter of the CNT and NP. We have explained this mismatch by the reshaping of catalyst NP before the growth of the CNT. In order to confirm this, we carefully removed the CNT with a tape from some samples after growth and performed AFM on these particles. The AFM inspections of Fig. 14a–f confirms clearly the reshaping of the catalyst NP during or before the growth. The NP after growth for both the NH_3 and NH_3+H_2 experiments appear smaller than those before.

4. Conclusions

The H_2 exposure during the annealing leads to formation of higher uniformity in diameter of catalyst NP than the other annealing gases NH_3 and $H_2 + NH_3$. The H_2 determines the smallest catalyst NP with mean diameters between 11 and 12 nm. For NH_3 annealed NP they are 18–20 nm, and 17–18 nm for $NH_3 + H_2$. NH_3 is not proper to form spherical NP suitable for the CNT growth because the NP appear like big clusters. NP with mean diameters of 20 nm were obtained with two annealing steps (NH_3 and H_2). They have the same diameter range of NH_3, but they are well-defined spherical NP (not clusters). Longer annealing times (10–300 s) don't change significantly the dimensions of the annealed $NH_3 + H_2$ and NH_3 catalyst NP. From all our CNT inspections, their diameters don't seem to exceed 15 nm and thus the CNT diameter doesn't increase when the catalyst NP become larger. This could be due to a reshaping of the catalyst NP becoming smaller during the first exposure of C_2H_2 before the CNT growth. The time taken to reshape the NP (time frame of the fixed growth time of 100 s) could be the reason for the height reduction. Longer annealing times with H_2 exposure improves the alignment of the CNT. In this case the alignment doesn't increase the height. H_2 during the annealing promotes the growth of more aligned CNT than the other annealed with NH_3 or NH_3 +H_2 and the alignment of the CNT is supported by the growth of the CNT in bundles.

CRediT authorship contribution statement

R. Pezone: Conceptualization, Methodology, Investigation, Writing - original draft, Writing - review & editing, Visualization. **S. Vollebregt:** Conceptualization, Supervision. **P.M. Sarro:** Project administration, Funding acquisition. **S. Unnikrishnan:** Project administration, Supervision, Funding acquisition.

Declaration of competing interest

The authors declare that they have no known competing financial interests or personal relationships that could have appeared to influence the work reported in this paper.

Acknowledgments

The authors would like to thank the Delft University of Technology Else Kooi Lab and the Holst Centre staff.

References

[1] E. Frackowiak, F. Béguin, Carbon materials for the electrochemical storage of energy in capacitors, Carbon 39 (6) (2001) 937–950, https://doi.org/10.1016/S0008-6223(00)00183-4.
[2] Z. Xiong, Y.S. Yun, H.J. Jin, Applications of carbon nanotubes for lithium ion battery anodes, Materials 6 (2013) 1138–1158, https://doi.org/10.3390/ma6031138.
[3] P. Fabian, A. Holger, S. Benjamin, K. Stefan, Nanostructured networks for energy storage: vertically aligned carbon nanotubes (VACNT) as current collectors for high-power Li4Ti5O12(LTO)//LiMn2O4(LMO) lithium-ion batteries, Batteries 3 (37) (2017) 1–14, https://doi.org/10.3390/batteries3040037.
[4] M. Notarianni, J. Liu, K. Vernon, N. Motta, Synthesis and applications of carbon nanomaterials for energy generation and storage, Beilstein J. Nanotechnol. 7 (2016) 149–196, https://doi.org/10.3762/bjnano.7.17.
[5] S. Esconjauregui, B.C. Bayer, M. Fouquet, C.T. Wirth, F. Yan1, R. Xi, et al., Use of plasma treatment to grow carbon nanotube forests on TiN substrate, J. Appl. Phys. 109 (2011) 114312, https://doi.org/10.1063/1.3587234.
[6] J. Daewoong, K. Jae-Hak, L. Kyung, L.J. Overzet, G. Lee, Effects of pre-annealing of Fe catalysts on growth of spin-capable carbon nanotubes, Diam. Relat. Mater. 38 (2013) 87–92, https://doi.org/10.1016/j.diamond.2013.06.021.
[7] M. Bedewy, B. Viswanath, E.R. Meshot, D.N. Zakharov, E.A. Stach, A.J. Hart, Measurement of the dewetting, nucleation, and deactivation kinetics of carbon nanotube population growth by environmental transmission electron microscopy, Chem. Mater. 28 (11) (2016) 3804–3813, https://doi.org/10.1021/acs.chemmater.6b00798.
[8] S. Min Kim, C.L. Pint, P.B. Amama, D.N. Zakharov, Robert H. Hauge, B. Maruyama, et al., Evolution in catalyst morphology leads to carbon nanotube growth termination, J. Phys. Chem. Lett. 1 (6) (2010) 918–922, https://doi.org/10.1021/jz9004762.
[9] S. Sakurai, H. Nishino, D.N. Futaba, S. Yasuda, T. Yamada, A. Maigne, et al., Role of subsurface diffusion and Ostwald ripening in catalyst formation for single-walled carbon nanotube forest growth, J. Am. Chem. Soc. 134 (4) (2012) 2148–2153, https://doi.org/10.1021/ja208706c.
[10] P.B. Amama, C.L. Pint, L. McJilton, S.M. Kim, E.A. Stach, P.T. Murray, et al., Role of water in super growth of single-walled carbon nanotube carpets, Nano Lett. 9 (1) (2009) 44–49, https://doi.org/10.1021/nl801876h.
[11] K. Hasegawa, S. Noda, Moderating carbon supply and suppressing Ostwald ripening of catalyst particles to produce 4.5-mm-tall single-walled carbon nanotube forests, Carbon 49 (13) (2011) 4497–4504, https://doi.org/10.1016/j.carbon.2011.06.061.
[12] G.D. Nessim, A.J. Hart, J.S. Kim, D. Acquaviva, J. Oh, C.D. Morgan, et al., Tuning of vertically-aligned carbon nanotube diameter and areal density through catalyst pre-treatment, Nano Lett. 8 (11) (2008) 3587–3593, https://doi.org/10.1021/nl801437c.
[13] S. Sakurai, M. Inaguma, D.N. Futaba, M. Yumura, K. Hata, Diameter and density control of single-walled carbon nanotube forests by modulating Ostwald ripening through decoupling the catalyst formation and growth processes, Small 9 (21) (2013) 3584–3592, https://doi.org/10.1002/smll.201300223.
[14] R.H. Poelma, B. Morana, S. Vollebregt, E. Schlangen, H.W. van Z, F. Xuejun, G.Q. Zhang, Tailoring the mechanical properties of high-aspect-ratio carbon nanotube Arrays using amorphous silicon carbide coatings, Adv. Funct. Mater. 24 (36) (2014) 5737–5744, https://doi.org/10.1002/adfm.201400693.
[15] S. Chakrabarti, T. Nagasaka, Y. Yoshikawa, L. Pan, Yoshikazu Nakayama, Growth of super long aligned brush-like carbon nanotubes, Jpn. J. Appl. Phys. 45 (28) (2006) L720–L722.
[16] G. Zhong, T. Iwasaki, J. Robertson, Hiroshi Kawarada, Growth kinetics of 0.5 cm vertically aligned single-walled carbon nanotubes, J. Phys. Chem. B 11 (8) (2007) 1907–1910.
[17] M. Cantoro, S. Hofmann, S. Pisana, V. Scardaci, A. Parvez, C. Ducati, A. Ferrari, et al., Catalytic chemical vapor deposition of single - wall carbon nanotubes at low temperatures, Nano Lett. 6 (6) (2006) 1107–1112. American Chemical Society.
[18] S. Sakurai, H. Nishino, D.N. Futaba, S. Yasuda, T. Yamada, A. Maigne, Y. Matsuo, et al., Role of subsurface diffusion and Ostwald ripening in catalyst formation for single-walled carbon nanotube forest growth, J. Am. Chem. Soc. 134 (2012) 2148–2153.
[19] H. Ago, T. Ayagaki, Y. Ogawa, M. Tsuji, Ultrahigh-vacuum-assisted control of metal nanoparticles for horizontally aligned single-walled carbon nanotubes with extraordinary uniform diameters, J. Phys. Chem. C 115 (27) (2011) 13247–13253, https://doi.org/10.1021/jp2038448.
[20] Y. Wang, Z. Luo, B. Li, P.S. Ho, Z. Yao, L. Shi, et al., Comparison study of catalyst nanoparticle formation and carbon nanotube growth: support effect, J. Appl. Phys. 101 (12) (2007), https://doi.org/10.1063/1.2749412, 124310.
[21] C. Mattevi, C.T. Wirth, S. Hofmann, R. Blume, M. Cantoro, C. Ducati, et al., In-situ X-ray photoelectron spectroscopy study of Catalyst–Support interactions and growth of carbon nanotube forests, J. Phys. Chem. C 112 (32) (2008) 12207–12213, https://doi.org/10.1021/jp802474g.
[22] M. Xu, D.N. Futaba, M. Yumura, K. Hata, Alignment control of carbon nanotube forest from random to nearly perfectly aligned by utilizing the crowding effect, ACS Nano 6 (7) (2012) 5837–5844, https://doi.org/10.1021/nn300142j.
[23] Y. Taek Jang, J.H. Ahn, Y.H. Lee, B.K. Ju, Effect of NH3 and thickness of catalyst on growth of carbon nanotubes using thermal chemical vapor deposition, Chem. Phys. Lett. 372 (5–6) (2003) 745–749, https://doi.org/10.1016/S0009-

2614(03)00501-3.
[24] G. Chen, R.C. Davis, D.N. Futaba, S. Sakurai, K. Kobashi, et al., A sweet spot for highly efficient growth of vertically aligned single-walled carbon nanotube forests enabling their unique structures and properties, Nanoscale 8 (2016) 162–171, https://doi.org/10.1039/c5nr05537g.
[25] C. Lu, J. Liu, Controlling the diameter of carbon nanotubes in chemical vapor deposition method by carbon feeding, J. Phys. Chem. B 110 (41) (2006) 20254–20257, https://doi.org/10.1021/jp0632283.
[26] D. Moszyński, I. Moszyńska, W. Arabczyk, Iron nitriding and reduction of iron nitrides in nanocrystalline Fe–N system, Mater. Lett. 78 (2012) 32–34, https://doi.org/10.1016/j.matlet.2012.03.047.
[27] C.T. Wirth, B.C. Bayer, A.D. Gamalski, S. Esconjauregui, R.S. Weatherup, C. Ducati, C. Baehtz, et al., The phase of iron catalyst nanoparticles during carbon nanotube growth, Chem. Mater. 24 (2012) 4633–4640, https://doi.org/10.1021/cm301402g.